Measurement 214 (2023) 112759

Contents lists available at ScienceDirect

Measurement

journal homepage: www.elsevier.com/locate/measurement

Identification of modal parameters of a model turbine blade with a curved surface under random excitation with a three-dimensional continuously scanning laser Doppler vibrometer system

K. Yuan, W.D. Zhu *

Department of Mechanical Engineering, University of Maryland, Baltimore County, 1000 Hilltop Circle, Baltimore, MD 21250, United States

ARTICLE INFO

Keywords:
General-purpose 3D CSLDV system
Curved surface
Extended demodulation method
Turbine blade
3D modal parameter identification

ABSTRACT

Modal parameters of a model turbine blade with a curved surface excited by white noise are identified by a novel general-purpose 3D continuously scanning laser Doppler vibrometer (CSLDV) system via an extended demodulation method (EDM). The proposed general-purpose system is calibrated to synchronously and continuously move three laser spots on the curved surface of the blade along the same scan trajectory and capture its 3D vibrations. The EDM is used to estimate its damped natural frequencies (DNFs) and 3D full-field undamped mode shapes. Identified modal parameters are compared with those from a commercial 3D scanning laser Doppler vibrometer (SLDV) system. Differences between their first six DNFs are less than 1.5%; their first six mode shapes are highly correlated as their modal assurance criterion values all exceed 95%. However, the 3D CSLDV system has much higher efficiency in obtaining 3D mode shapes of the blade than the 3D SLDV system.

1. Introduction

It is important to measure three-dimensional (3D) full-field vibration of a structure in structural dynamic analysis and structural health monitoring (SHM), especially for such structures as turbine blades and pipelines, which have complex, curved surfaces. 3D full-field vibration measurement of a complex structure can improve accuracy of its SHM by providing more information to detect damage in it than single-axis or one-dimensional (1D) vibration measurement [1]. It can also benefit product design of a complex structure by matching its modal parameters from its modal test [2] and those from its finite element (FE) analysis [3,4].

A triaxial accelerometer can be attached on a structure to measure its 3D vibrations, which can lead to mass loading, especially when multiple triaxial accelerometers are needed in modal tests of light-weight structures [5]. For large structures such as long-span bridges, the mass loading from accelerometers can have fewer effects on measured response. For example, methods were developed to accurately identify natural frequencies and mode shapes of bridges under ambient excitation [6–8]. As a non-contact sensor, a laser Doppler vibrometer (LDV) can be used to measure vibration of a structure by avoiding the mass loading problem. A conventional LDV can be used to measure 1D vibration of a test structure along the laser beam, but one needs to manually move it after completing measurement at one point. It can be extended and automated by mounting two orthogonal scan mirrors in front of its laser, which can be referred to as a scanning laser Doppler vibrometer (SLDV). Some studies aimed to extend the LDV and SLDV from one dimension to three dimensions. Investigations include robotizing a LDV using a 6-axis robot arm and combining a SLDV with a multi-axis positioning frame [9,10], sequentially moving a LDV or SLDV to three independent locations [11–13], and using three LDVs or SLDVs to synchronously measure vibrations at the same point [14], which has been commercialized as 3D vibration measurement products, e.g., a Polytec PSV-500 system. Researchers and engineers have applied these systems in various areas, such as obtaining longitudinal vibration shapes of a beam to detect its damage [15], validating FE models of complex structures [16,17], updating the FE model of a fan blade using its measured 3D dynamic strain distributions [18], and analyzing 3D vibration behaviors of power tools to reduce their operating noise [19]. However, in 3D SLDV measurement, laser spots can only be moved from one point to the next on a pre-designed measurement grid in a step-wise manner, which can lead to a long test time, especially when the test area is large and the measurement grid is dense [1].

One approach for saving the test time is to develop a 1D continuously

* Corresponding author.
E-mail addresses: kyuan1@umbc.edu (K. Yuan), wzhu@umbc.edu (W.D. Zhu).

https://doi.org/10.1016/j.measurement.2023.112759
Received 11 January 2023; Received in revised form 1 March 2023; Accepted 19 March 2023
Available online 23 March 2023

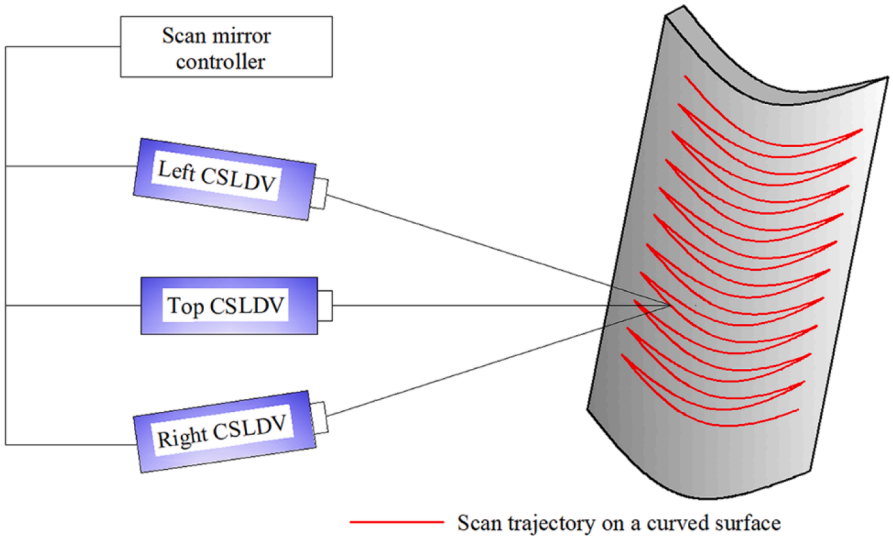

Fig. 1. Main modules for running the general-purpose 3D CSLDV system.

scanning laser Doppler vibrometer (CSLDV) whose laser spot can continuously scan the surface of the test structure via controlling its scan mirrors [20,21]. The 1D CSLDV can be used in many areas, such as transverse vibration measurement and modal testing of structures [21–23], and their damage detection [24–27]. However, investigations about using a CSLDV to measure 3D velocity components of a structure are still scarce. A vibration measurement system using the CSLDV and capturing 3D operational deflection shapes of a turbine blade excited by a multi-frequency signal was developed by Weekes and Ewins [28]. The CSLDV was moved to three independent locations during their test. It is a main challenge to have scan trajectories of the CSLDV at three locations to be exactly the same. Also, it is not possible to deal with transient response of a structure under random excitation and estimate its 3D mode shapes using the single CSLDV, since acquisition of three velocity components is not simultaneous. In addition, it takes much time to reset the CSLDV three times during measurement. Recently, a novel 3D vibration measurement system was built using three laser heads and an external controller to address the above challenges, which can be referred to as a 3D CSLDV system [29–31]. Three laser spots in the system can be aligned via a calibration procedure, and synchronously and continuously moved along the same scan trajectory. Accuracy of the system was validated via modal tests of beams and plates whose estimated 3D modal parameters were compared with those from their FE analyses and a commercial Polytec PSV-500-3D system. A limitation of the system is that it can only be used to scan structures with planar surfaces. However, surfaces of real structures in engineering practices can be curved. Yuan and Zhu [32] recently developed a novel general-purpose 3D CSLDV system to measure operational deflection shapes of a turbine blade under sinusoidal excitation. Operational deflection shapes obtained by the system were compared with corresponding results from a commercial SLDV system to validate its accuracy through high modal assurance criterion (MAC) values. Further investigations are needed to estimate modal parameters, such as damped natural frequencies (DNFs) and 3D undamped mode shapes (UMSs), of a structure with a curved surface excited by white noise, which is the most realistic excitation. It can be expected that response of structures under random excitation has much more noise than that under sinusoidal excitation, meaning that it is more challenging to identify their UMSs under random excitation than their operational deflection shapes under sinusoidal excitation.

Several methods including the demodulation method, polynomial method, and lifting method have been developed and improved to process signals from CSLDV measurements. By using these methods, one can identify modal parameters of structures under various excitations, such as sinusoidal [33], impact [34,35], multi-sine [36,37], and ambient excitations [23,30,38,39]. The conventional demodulation method cannot be used to process measured response of a structure under random excitation since a known excitation frequency is needed to conduct demodulation. An improved demodulation method was developed to estimate modal parameters of a rotating fan blade under ambient excitation using a tracking CSLDV through 1D and two-dimensional (2D) scan trajectories [23,39]; however, these studies focused on transverse mode shape identification. Yuan and Zhu [30] developed a 3D CSLDV system in conjunction with an extended demodulation method (EDM) to identify DNFs and 3D UMSs of a beam excited by white noise. However, the test beam in Ref. [30] has a planar surface and the scan trajectory is a straight line. One still needs to investigate how the 3D CSLDV system can be used with the EDM on a structure excited by white noise when it has a curved surface.

This work aims to identify 3D modal parameters of a model turbine blade with a curved surface excited by white noise using the novel general-purpose 3D CSLDV system via the EDM. Three laser heads, an external controller, and a profile scanning unit are used to build the 3D CSLDV system. In order to ensure that three laser spots can synchronously and continuously move along the same scan trajectory, spatial relations among the three laser heads are determined via a calibration procedure, and used with the 3D profile of the turbine blade to design a 3D full-field trajectory to scan its surface. The proposed EDM is an operational modal analysis method that can be used to process measured response of the turbine blade under random excitation to obtain its DNFs and 3D full-field UMSs (FF-UMSs). Bandpass filtering and data averaging were conducted in the EDM for enhancing the signal-to-noise ratio (SNR) of measured response. The identified first six modal parameters of the turbine blade are compared with those from a commercial 3D SLDV system. Differences between their first six DNFs are less than 1.5%, and their first six mode shapes are highly correlated as their MAC values all exceed 95%. The number of points scanned by the 3D CSLDV system is about 1,500 times that by the 3D SLDV system, while the test time consumed by the 3D CSLDV system is less than 1/8 of that by the 3D SLDV system. A significant advancement of this work is that the general-purpose 3D CSLDV system can process measured response of a structure with a curved surface excited by white noise via the EDM to estimate its DNFs and 3D FF-UMSs.

This paper proposes an innovative method, namely the EDM, which can be used with a novel general-purpose 3D CSLDV system to identify 3D modal parameters of a structure with a curved surface under random

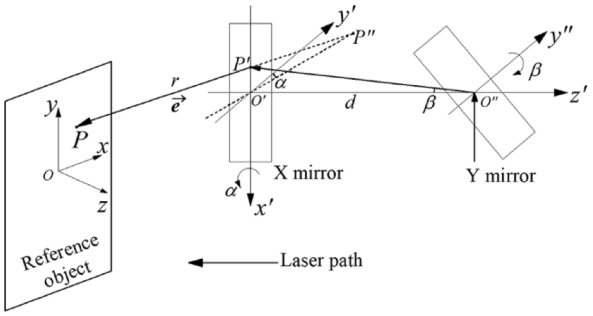

Fig. 2. Orthogonally mounted scan mirrors and their spatial relations with respect to the reference object.

excitation. The proposed EDM is different from previous methods used for CSLDV measurement since it integrates bandpass filtering and data averaging to enhance the SNR of measured response and accurately identify modal parameters of the structure with a curved surface. The remainder of the paper is structured as follows. The methodology for calibrating the proposed general-purpose system is shown in Section 2.1; methods for designing a 3D zig-zag scan trajectory, constructing the velocity transformation from vibrometer coordinate systems (VCSs) to the measurement coordinate system (MCS), and processing measured response via the EDM are shown in Sections 2.2, 2.3, and 2.4, respectively. The experimental setup of the clamped turbine blade for estimating its DNFs and 3D FF-UMSs is shown in Section 3.1, results of the 3D profile of the turbine blade and generated mirror signals are shown in Section 3.2, and details of transforming measured velocity from VCSs to the MCS and estimating 3D modal parameters of the turbine blade using the EDM are shown in Sections 3.3 and 3.4, respectively. Main Conclusions are shown in Section 4.

2. General-purpose 3D CSLDV system in conjunction with the EDM

Main components of the proposed general-purpose 3D CSLDV system are shown in Fig. 1. Its three laser heads, which can be referred to as Top, Left, and Right laser heads, are extended from the commercial Polytec PSV-500 3D SLDV system and used for vibration data acquisition. A dSPACE MicroLabBox controller is integrated with the 3D SLDV system that only has a step scanning function to conduct a continuously scanning mode. Spatial relations among three laser heads can be determined using a reference object via a calibration procedure and used with the 3D profile of a test structure to pre-design a 3D full-field trajectory to scan its curved surface. Input signals of scan mirrors with respect to the scan trajectory can make three laser spots to scan it in a synchronous and continuous mode.

2.1. Methodology for system calibration

The MCS is built using a reference object, as shown in the Appendix, which can provide multiple calibration points with known coordinates. There are twenty-one points on the plane of the reference object and eight points on its two poles. Three VCSs of three laser heads are based on their respective orthogonally mounted scan mirrors, whose geometrical model can be seen in Fig. 2. X and Y mirrors rotate about orthogonal axes $o'x'$ and $o''y''$, respectively, and both of their rotating centers, o' and o'', are on $o'z'$, whose separation distance is d. The point P'' is the virtual image of the point o'', which means that $|o'P''| = |o'o''| = d$. The generated laser beam passes through X and Y mirrors at incident points P' and o'', respectively. The distance between the point P' and a point P on the reference object is r. In the VCS, coordinates of points P' and P'' are written as

$$\mathbf{P}'_{VCS} = [-d\tan(\beta), 0, 0]^{\mathrm{T}} \tag{1}$$

$$\mathbf{P}''_{VCS} = [0, d\cos(\alpha), d\sin(\alpha)]^{\mathrm{T}} \tag{2}$$

respectively, where α and β denote rotating angles of X and Y mirrors, respectively, and the subscript T denotes transpose of a matrix. The unit vector of PP' can be derived as

$$\begin{aligned}\mathbf{e} = \frac{P'P''}{|P'P''|} &= \frac{1}{d\sqrt{\tan^2(\beta)+1}}[d\tan(\beta), d\cos(\alpha), d\sin(\alpha)]^{\mathrm{T}} \\ &= [\sin(\beta), \cos(\alpha)\cos(\beta), \sin(\alpha)\cos(\beta)]^{\mathrm{T}}\end{aligned} \tag{3}$$

Coordinates of a selected calibration point P on the reference objective can be written using the VCS as

$$\begin{aligned}\mathbf{P}_{VCS} = \mathbf{P}'_{VCS} - r\mathbf{e} &= [-d\tan(\beta), 0, 0]^{\mathrm{T}} - r[\sin(\beta), \cos(\alpha)\cos(\beta), \sin(\alpha)\cos(\beta)]^{\mathrm{T}} \\ &= [-d\tan(\beta) - r\sin(\beta), -r\cos(\alpha)\cos(\beta), -r\sin(\alpha)\cos(\beta)]^{\mathrm{T}}\end{aligned} \tag{4}$$

The relation between coordinates of P in the MCS $\mathbf{P}_{MCS}$ and the VCS $\mathbf{P}_{VCS}$ can be written as

$$\mathbf{P}_{MCS} = \mathbf{T} + \mathbf{R}\mathbf{P}_{VCS} \tag{5}$$

where $\mathbf{P}_{MCS} = [x, y, z]^{\mathrm{T}}$ can be directly read from the reference object, $\mathbf{T} = [x_{o'}, y_{o'}, z_{o'}]^{\mathrm{T}}$ denotes coordinates of o' in the MCS, and $\mathbf{R}$ is the direction cosine matrix from the MCS to the VCS. By using the method proposed in Refs. [29] and [40], which includes procedures of solving an over-determined nonlinear problem and an optimization problem, three pairs of $\mathbf{T}$ and $\mathbf{R}$ matrices for the system can be calculated. More details about the calibration method can be found in the Appendix.

To evaluate the accuracy of estimated $\mathbf{T}$ and $\mathbf{R}$ matrices for three laser heads, a calibration error is defined as the distance between the calibration point and the laser spot, which can be written as

$$\delta^m = \left\| \mathbf{P}^m_{MCS} - \left(\mathbf{T} + \mathbf{R}\mathbf{P}^m_{VCS}\right) \right\| \tag{6}$$

where the superscript m denotes the index of calibration points, whose maximum value is six in this work as shown in the Appendix. Mean values of calibration errors from all six calibration points are 505.9 μm, 403.5 μm, and 452.5 μm for Top, Left, and Right laser heads, respectively. Stand-off distances of the three laser heads are about 2100 mm during measurement in this work, which means that diameters of laser spots are about 490 μm. One can see that calibration errors and the size of laser spots are of the same order, indicating that positions of three laser heads in the MCS are accurately calculated through the calibration procedure.

2.2. Methodology for designing a 3D zig-zag scan trajectory

In Refs. [30] and [31], a multi-bisection method based on an assumption of a planar geometry was used in scan trajectory designs for a straight beam and a flat plate. Although the method is efficient, it is not suitable for scan trajectory designs for structures with curved surfaces. To address the above challenge, a method for designing 3D scan trajectories is developed for general surfaces, including both planar and curved ones.

Three VCSs and one MCS have been introduced in Section 2.1. Since a measurement point P^k in the MCS has the same coordinates, their coordinates in three VCSs are different. Therefore, one has

$$\mathbf{P}^k_{MCS} = \mathbf{T}_1 + \mathbf{R}_1\mathbf{P}^k_{VCS\_1} = \mathbf{T}_2 + \mathbf{R}_2\mathbf{P}^k_{VCS\_2} = \mathbf{T}_3 + \mathbf{R}_3\mathbf{P}^k_{VCS\_3} \tag{7}$$

where subscripts 1, 2, and 3 denote Top, Left, and Right laser heads, respectively, and the superscript k is the index of the measurement point on the surface. Coordinates in the MCS $\mathbf{P}_{MCS}$ of all measurement points on the surface can be obtained using a 3D profile scanner that is an

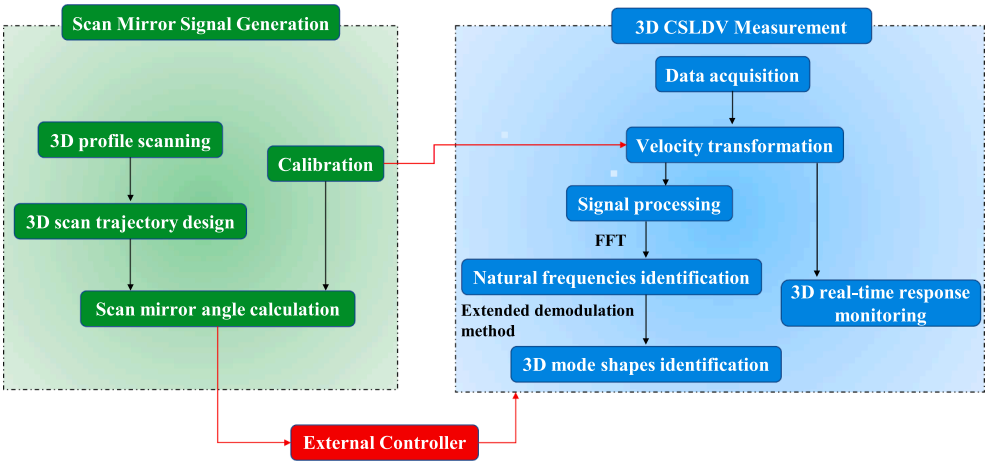

Fig. 3. Main steps of scan mirror signal generation and 3D CSLDV measurement.

internal unit of the Polytec PSV-500-3D system. Therefore, the 3D profile scanner and three laser heads are in the same coordinate system with respect to the same reference object, and errors from interaction between devices can be reduced to a relatively low level. The original 3D profile of the test structure can be processed by a linear interpolation method to obtain a much denser measurement grid that can be inputted into scan mirrors to make them to continuously rotate. Coordinates of the point P^k in three VCSs are

$$\mathbf{P}^k_{VCS\_1} = \mathbf{R}_1^{-1}\left(\mathbf{P}^k_{MCS} - \mathbf{T}_1\right) \tag{8a}$$

$$\mathbf{P}^k_{VCS\_2} = \mathbf{R}_2^{-1}\left(\mathbf{P}^k_{MCS} - \mathbf{T}_2\right) \tag{8b}$$

$$\mathbf{P}^k_{VCS\_3} = \mathbf{R}_3^{-1}\left(\mathbf{P}^k_{MCS} - \mathbf{T}_3\right) \tag{8c}$$

By Eq. (4), one has rotating angles of three laser heads

$$\begin{aligned} \alpha_1^k &= \arctan\left(z^k_{VCS\_1}/y^k_{VCS\_1}\right) \\ \beta_1^k &= \arctan\left(x^k_{VCS\_1}/\left(y^k_{VCS\_1}/\cos\left(\alpha_1^k\right) - d\right)\right), \end{aligned} \tag{9a}$$

$$\begin{aligned} \alpha_2^k &= \arctan\left(z^k_{VCS\_2}/y^k_{VCS\_2}\right) \\ \beta_2^k &= \arctan\left(x^k_{VCS\_2}/\left(y^k_{VCS\_2}/\cos\left(\alpha_2^k\right) - d\right)\right), \end{aligned} \tag{9b}$$

$$\begin{aligned} \alpha_3^k &= \arctan\left(z^k_{VCS\_3}/y^k_{VCS\_3}\right) \\ \beta_3^k &= \arctan\left(x^k_{VCS\_3}/\left(y^k_{VCS\_3}/\cos\left(\alpha_3^k\right) - d\right)\right). \end{aligned} \tag{9c}$$

2.3. Methodology for the velocity transformation among coordinate systems

By synchronously and continuously moving three laser spots along a pre-designed scan trajectory, velocities in three VCSs can be directly acquired in one measurement. To transform them to vibration components in the MCS, the following equation can be established using calculated direction cosine matrices and unit vectors:

$$\left[V_x, V_y, V_z\right]^{\mathrm{T}} = \left[\left[\mathbf{R}_1\mathbf{e}_1, \mathbf{R}_2\mathbf{e}_2, \mathbf{R}_3\mathbf{e}_3\right]^{\mathrm{T}}\right]^{-1}\left[V_1, V_2, V_3\right]^{\mathrm{T}} \tag{10}$$

where V_1, V_2, and V_3 are directly acquired velocities from Top, Left, and Right laser heads, respectively, and V_x, V_y, and V_z are transformed velocity components along three directions of the MCS, respectively. The obtained real-time 3D velocity components can be used to not only monitor the test structure in its operating condition, but also estimate its DNFs and 3D FF-UMSs via a signal processing procedure.

2.4. EDM for 3D CSLDV measurement of a structure under random excitation

The governing partial differential equation of a linear, time-invariant, viscously damped structure under external excitation can be solved to obtain its response at a spatial position $\mathbf{x}$ [30,41]:

$$u(\mathbf{x},t) = \sum_{i=1}^{N} \phi_i(\mathbf{x})\phi_i(\mathbf{x}_p)\left[A_i(t)\cos\left(\omega_{d,i}t\right) + B_i(t)\sin\left(\omega_{d,i}t\right) + C_i(t)\right] \tag{11}$$

where $\mathbf{x}_p$ denotes the position of a concentrated force, t is time, N is the total number of points on the measurement grid, ϕ_i is the i-th mass-normalized eigenfunction of the associated undamped structure, $A_i(t)$, $B_i(t)$, and $C_i(t)$ are arbitrary functions of time related to the concentrated force, and $\omega_{d,i}$ is the i-th DNF of the structure that can be obtained by applying the fast Fourier transform (FFT) on response. Filtering the response u in Eq. (10) to allow $\omega_{d,i}$ to pass yields

$$u_i(\mathbf{x},t) = \Phi_i(\mathbf{x})\cos\left(\omega_{d,i}t - \varphi\right) = \Phi_{I,i}(\mathbf{x})\cos\left(\omega_{d,i}t\right) + \Phi_{Q,i}(\mathbf{x})\sin\left(\omega_{d,i}t\right) \tag{12}$$

where $\Phi_i(\mathbf{x})$ are responses with in-phase and quadrature components $\Phi_{I,i}(\mathbf{x})$ and $\Phi_{Q,i}(\mathbf{x})$, respectively, at measurement points along the scan trajectory, and φ is the phase variable. To obtain $\Phi_{I,i}(\mathbf{x})$ and $\Phi_{Q,i}(\mathbf{x})$, multiplying $u_i(\mathbf{x},t)$ in Eq. (11) by $\cos\left(\omega_{d,i}t\right)$ and $\sin\left(\omega_{d,i}t\right)$ yield

$$\begin{aligned} u_i(\mathbf{x},t)\cos\left(\omega_{d,i}t\right) &= \Phi_{I,i}(\mathbf{x})\cos^2\left(\omega_{d,i}t\right) + \Phi_{Q,i}(\mathbf{x})\sin\left(\omega_{d,i}t\right)\cos\left(\omega_{d,i}t\right) \\ &= \frac{1}{2}\Phi_{I,i}(\mathbf{x}) + \frac{1}{2}\Phi_{I,i}(\mathbf{x})\cos\left(2\omega_{d,i}t\right) + \frac{1}{2}\Phi_{Q,i}(\mathbf{x})\sin\left(2\omega_{d,i}t\right), \end{aligned} \tag{13}$$

$$\begin{aligned} u_i(\mathbf{x},t)\sin\left(\omega_{d,i}t\right) &= \Phi_{I,i}(\mathbf{x})\sin\left(\omega_{d,i}t\right)\cos\left(\omega_{d,i}t\right) + \Phi_{Q,i}(\mathbf{x})\sin^2\left(\omega_{d,i}t\right) \\ &= \frac{1}{2}\Phi_{Q,i}(\mathbf{x}) + \frac{1}{2}\Phi_{I,i}(\mathbf{x})\sin\left(2\omega_{d,i}t\right) - \frac{1}{2}\Phi_{Q,i}(\mathbf{x})\cos\left(2\omega_{d,i}t\right), \end{aligned} \tag{14}$$

respectively, where $\Phi_{I,i}(\mathbf{x})$ and $\Phi_{Q,i}(\mathbf{x})$ can be subsequently obtained by using a low-pass filter to remove $\sin\left(2\omega_{d,i}t\right)$ and $\cos\left(2\omega_{d,i}t\right)$. By applying the above procedure on the designed 3D zig-zag scan trajectory, the EDM in Ref. [30] is extended from one dimension to three dimensions and can be used to identify DNFs and 3D FF-UMSs of a turbine blade with a curved surface under random excitation. Corresponding steps are shown in Fig. 3.

3. Experimental validation

3.1. Testing setup of 3D CSLDV measurement

In this work, a model turbine blade was used as the test sample. It was manufactured from a trapezoidal plate with a thickness of 3.5 mm,

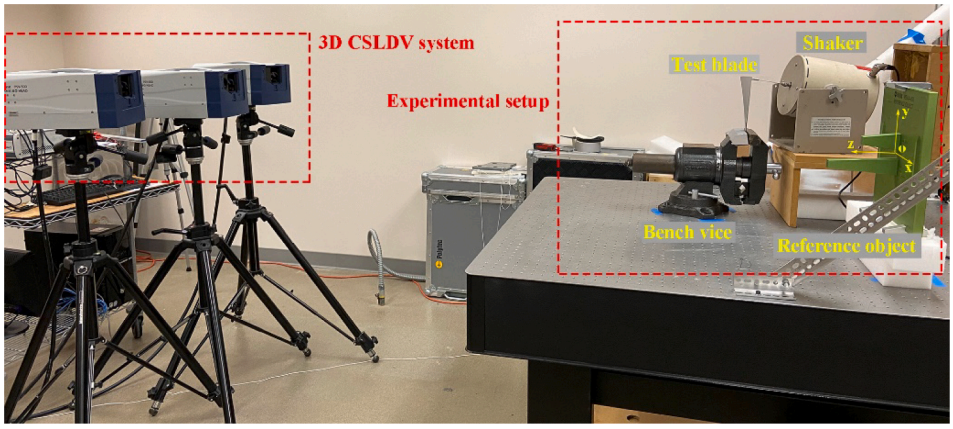

Fig. 4. Relative position of the model turbine blade and the 3D CSLDV system and details of the setup of the turbine blade including its boundary conditions and position in the MCS.

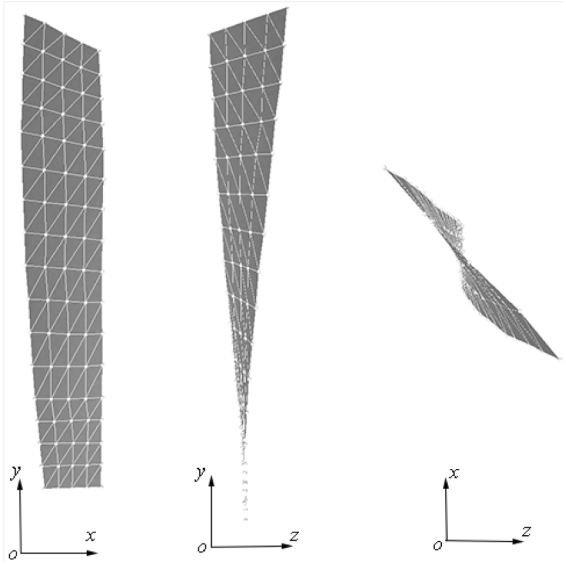

Fig. 5. Grid of measurement points and the 3D profile of the surface of the turbine blade.

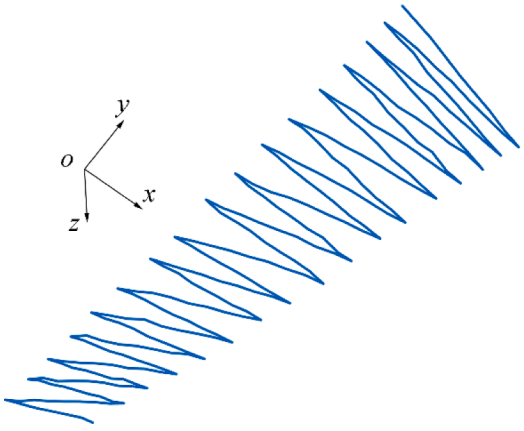

Fig. 6. 3D zig-zag scan trajectory pre-designed for the turbine blade to cover its full surface.

two bases of 42 mm and 26 mm, and an altitude of 173.9 mm via twisting, and used for methodology validation purposes. For vibration measurement, it does not matter whether the turbine blade is a real turbine blade or a model turbine blade, as the test procedure would be the same. One end of the turbine blade was viced onto a workbench to simulate its clamped-free boundaries. One can see from Fig. 4 that excitation was provided by a MODAL-50 shaker from MB Dynamics via a stinger attached on the free end of the turbine blade. Note that arrangement of three laser heads is close to a plane instead of a cone, as shown in Fig. 4, since modes of interest in this study are mostly bending or torsional modes, not longitudinal modes. To enhance signal intensity of laser spots, the turbine blade was covered by a reflective tape on its surface. As mentioned in Section 2, the MCS is determined by the reference object. As shown in Fig. 4, the turbine blade is parallel to the *o-xy* plane of the MCS built on the reference object, its out-of-plane vibration component is along the *z* direction, and its in-plane vibration components are along *x* and *y* directions. A periodic chirp signal whose frequency covers the range of 0 to 3000 Hz was used in the modal test of the turbine blade by the 3D SLDV system for 900 s, and a white-noise signal whose frequency covers the range of 0 to 3000 Hz was used as random excitation in its 3D CSLDV measurement for 115.5 s. Note that the difference between durations of periodic chirp and white-noise signals is due to different durations of the two systems to complete scanning of the whole surface of the turbine blade. The duration of the SLDV system includes times of sampling and moving laser spots, while the duration of the CSLDV system is determined by sampling and scanning frequencies of measurement, which will be discussed in Section 3.4.

This study aims to process response from 3D CSLDV measurement of a turbine blade with a curved surface under random excitation using the EDM, and to obtain its natural frequencies and 3D full-field mode shapes, so that a white-noise signal can be used as random excitation in 3D CSLDV measurement. Natural frequencies and mode shapes of the blade from 3D SLDV measurement were used as references to validate those from 3D CSLDV measurement. While modal parameters would not be affected by changes of excitation signals, it takes much less time in the SLDV test by using the periodic chirp signal than other excitation signals such as the white-noise signal that need many more averages. One advantage of the 3D CSLDV system over the 3D SLDV system is that it can save much test time. In order to show this feature, the periodic chirp signal that takes less time in SLDV measurement was selected as the excitation signal. In other words, the CSLDV system can still save much test time even when the SLDV system is in its best condition.

3.2. Results of mirror signal generation

Prior to design of the 3D scan trajectory, the 3D profile of the turbine

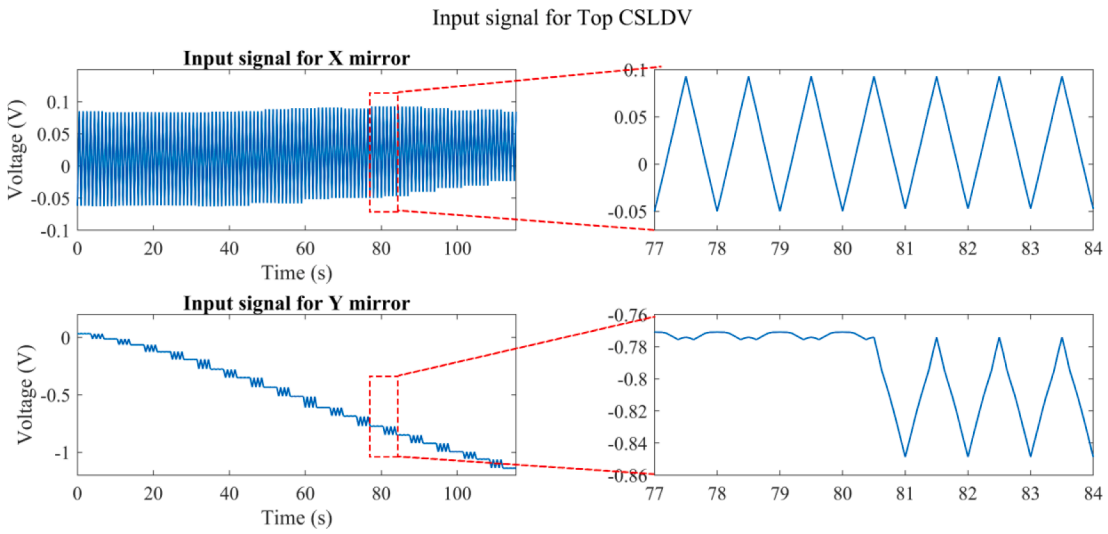

Fig. 7. Scan mirror signals for the Top CSLDV based on the 3D zig-zag scan trajectory in Fig. 6.

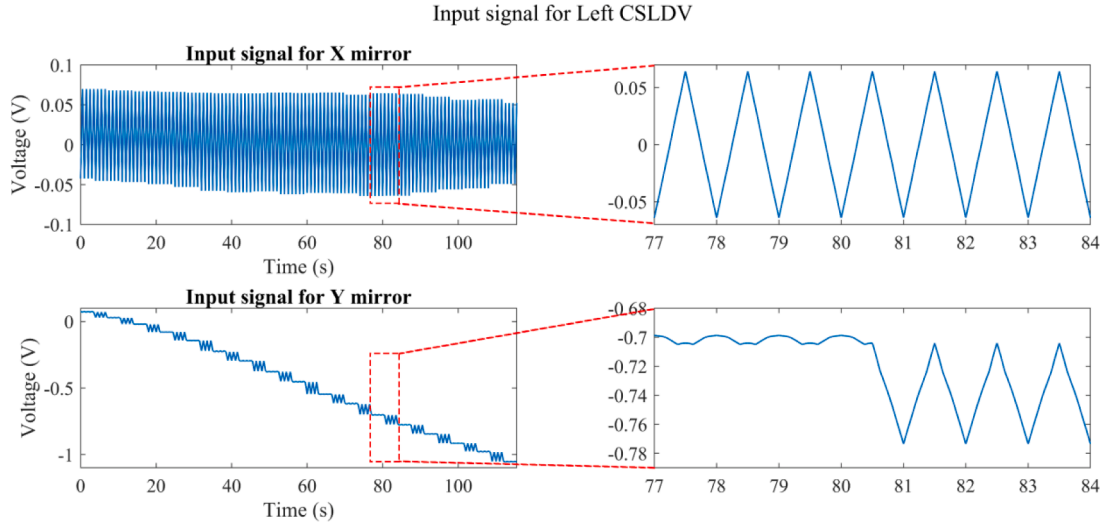

Fig. 8. Scan mirror signals for the Left CSLDV based on the 3D zig-zag scan trajectory in Fig. 6.

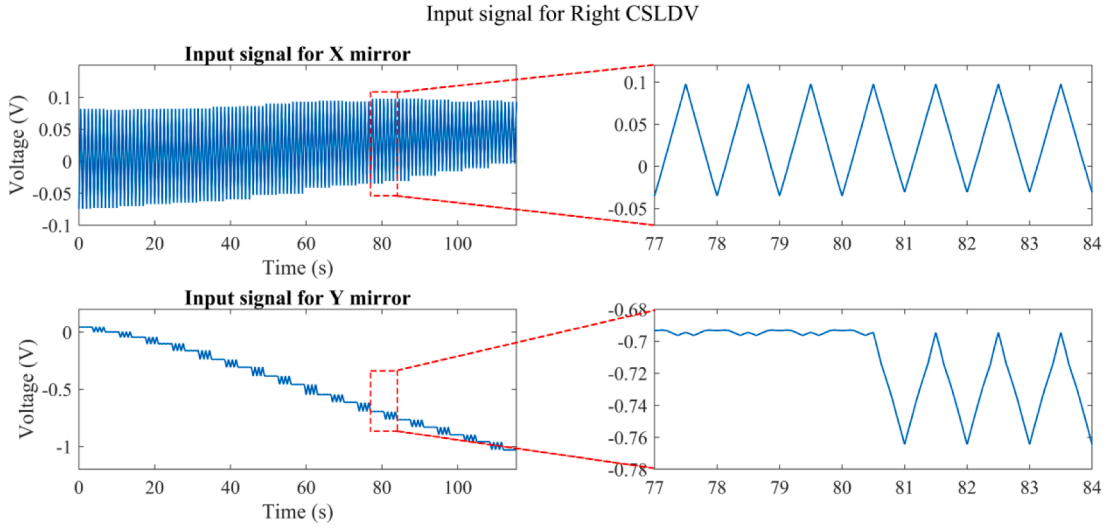

Fig. 9. Scan mirror signals for the Right CSLDV based on the 3D zig-zag scan trajectory in Fig. 6.

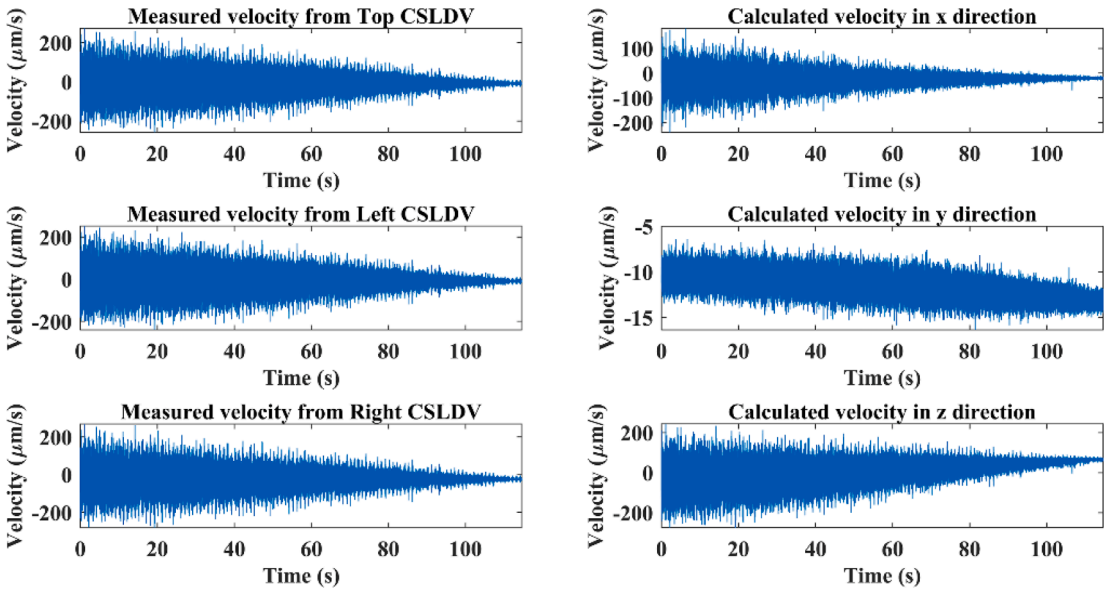

Fig. 10. Transformation from velocities measured in VCSs to three orthogonal components in the defined MCS.

Table 1
Comparisons between the consumed test time and the number of scanned points by the 3D CSLDV system and those by the 3D SLDV system.

Measurement method	3D CSLDV	3D SLDV
Consumed test time (s)	115.5	900
Number of scanned points	132,000	85

blade was measured. As shown in Fig. 5, a grid of 17×5 points were used as reference points for profile scanning and measurement points for SLDV measurement, and then linearly interpolated to be a denser grid that includes 33 scan lines for continuous scanning. The zig-zag scan trajectory, as shown in Fig. 6, was used since this study focused on processing response of a structure under random excitation using the EDM, and the zig-zag scan trajectory is more easily processed by the demodulation method than other scan trajectories. There are two main reasons for using the zig-zag trajectory in this work. First, for full-field CSLDV measurement on an area, a Lissajous trajectory or a zig-zag trajectory is commonly used, where the Lissajous trajectory is formed by two sine waves at different frequencies and the zig-zag trajectory is formed by two triangular waves at different frequencies [21]. The zig-zag trajectory scanning method can provide a uniform straight-line-based trajectory whose spatial position can be more easily and directly obtained using signals of two orthogonal scan mirrors than the Lissajous trajectory scanning method. The identified mode shapes can then be plotted in the 3D profile of the test structure. Therefore, the zig-zag trajectory fits this work better from the aspect of efficiency of scan trajectory design. Second, the signal processing method used in this work is based on signal demodulation that requires a low scan rate [21]. Additionally, data averaging conducted in this work requires laser spots to complete a few scan cycles on each scan line with a constant scan rate, which is difficult to achieve for the Lissajous trajectory. Therefore, the zig-zag trajectory fits this work better from the aspect of scan mirror control and signal processing.

In CSLDV measurement, the time of moving laser spots along a scan line for a full cycle can be defined as a scanning period T, and the scanning frequency $f_{sca} = 1/T$ is 1 Hz in this experiment. To denoise measured response, a three-time average was conducted for both 3D SLDV and CSLDV measurements. Therefore, it took $t = 33 \times 3.5 = 115.5$ s to conduct a full-field scan on the surface of the turbine blade, where 33 denotes the number of scan lines and 3.5 means the number of periods for each scan line, in which extra half periods were used to move laser spots to the end of a scan line to continue scanning on its next scan

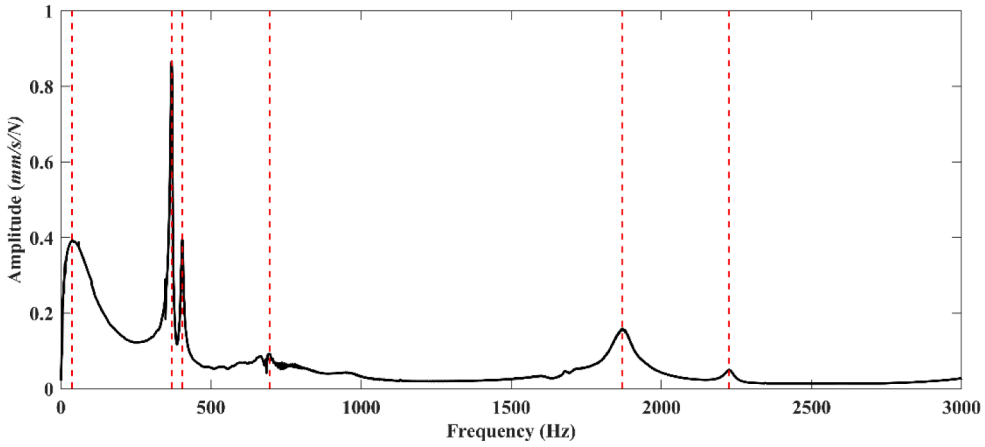

Fig. 11. DNFs of the turbine blade identified from the frequency spectrum measured by the 3D SLDV system, where the black solid line represents its frequency spectrum and red dashed lines mark its DNFs.

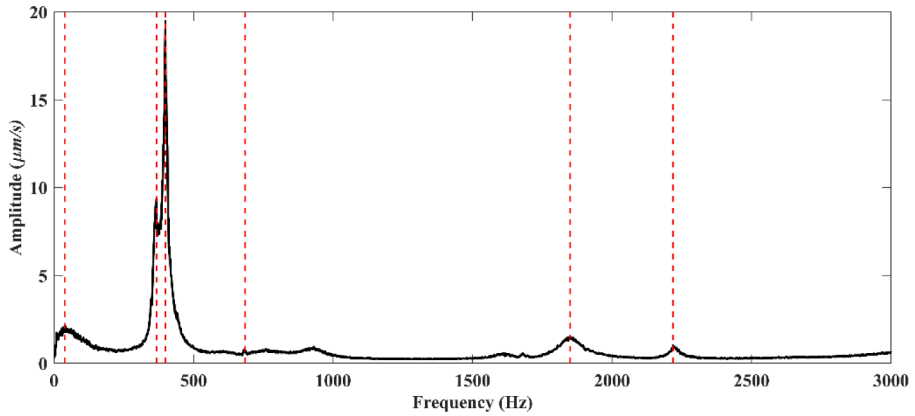

Fig. 12. DNFs of the turbine blade identified from the frequency spectrum measured by the 3D CSLDV system, where the black solid line represents its frequency spectrum and red dashed lines mark its DNFs.

Table 2
Comparison between the first six DNFs of the turbine blade identified by the two systems.

Mode No.	DNF (Hz)		Difference (%)
	3D CSLDV measurement	3D SLDV measurement	
1	38	37.5	1.3
2	367	370.5	0.9
3	399	403.3	1.1
4	685	695.1	1.5
5	1850	1870.8	1.1
6	2219	2226.3	0.3

line. Scan mirror signals of Top, Left, and Right laser heads can be found in Figs. 7-9, respectively, whose right subplots show details of two cycles. Time-voltage series for X and Y mirrors are triangular and curved, respectively, and much different from those in measurements of structures with planar surfaces [30,31].

3.3. Results of directly measured and transformed velocities

Directly measured vibrations in the experiment are in three VCSs of three laser heads, which can be transformed to three orthogonal velocity components in the same MCS using Eq. (9). Directly measured and transformed velocities of the turbine blade excited by white noise are shown in Fig. 10. Directly measured velocities in three VCSs and transformed velocities along three orthogonal axes in the MCS can be found in left and right subplots, respectively, where *y* axes are velocities

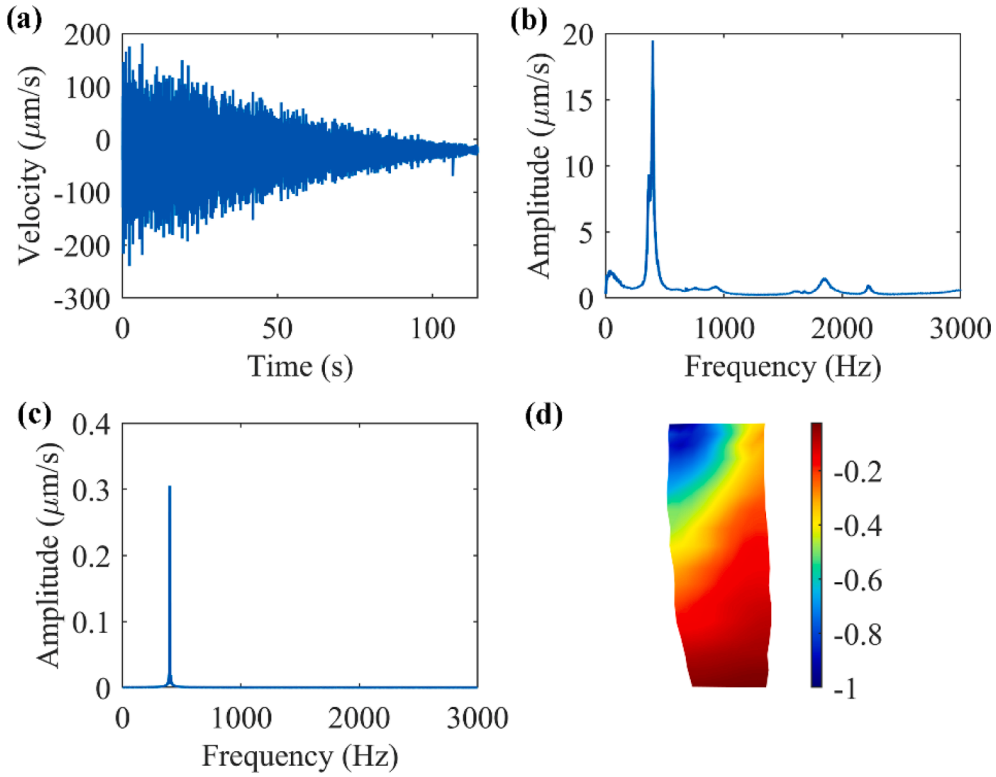

Fig. 13. Procedure of identifying the *x* component of the third 3D FF-UMS of the turbine blade: (a) the vibration component in the *x* direction of the MCS of the turbine blade, (b) the frequency spectrum of response in (a), (c) the frequency spectrum of response filtered by a bandpass filter with a passband of 398 to 400 Hz, where the only peak is the identified DNF of 399 Hz, and (d) the *x* component of the third FF-UMS of the turbine blade.

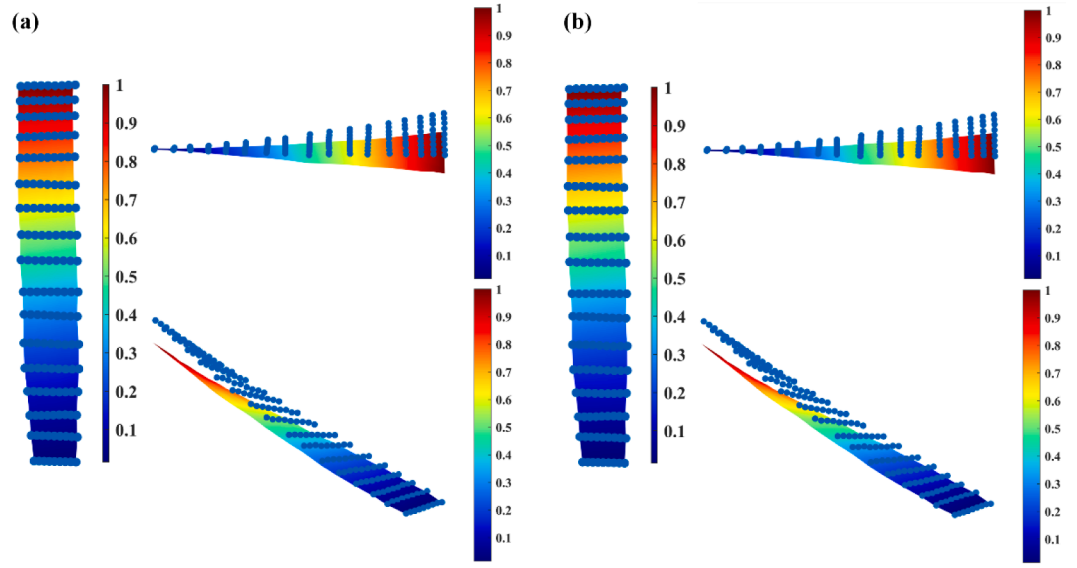

Fig. 14. (a) Estimated first FF-DMSs of the turbine blade using the 3D SLDV system and (b) corresponding FF-UMSs using the 3D CSLDV system, with views from three different angles.

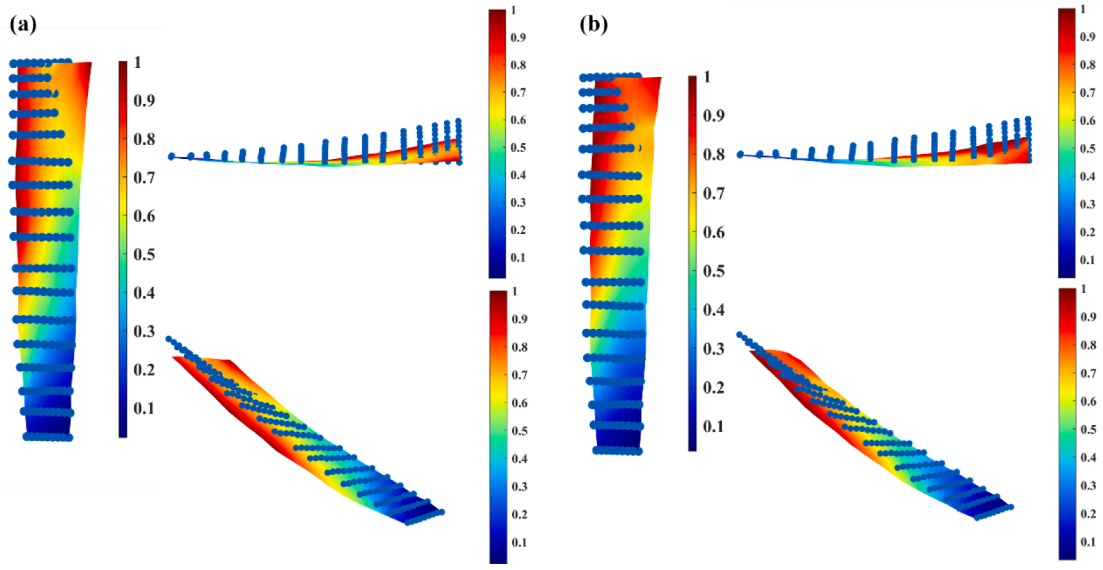

Fig. 15. (a) Estimated second FF-DMSs of the turbine blade using the 3D SLDV system and (b) corresponding FF-UMSs using the 3D CSLDV system, with views from three different angles.

and x axes are time. In Fig. 10, velocities at the beginning of time axes have much larger values than those at ends of time axes, since laser spots were moved from the free end of the turbine blade to its clamped end during measurement. Clamped-free boundaries of the turbine blade also led to a much smaller amplitude of the velocity along the y direction in the MCS than those along the other two directions. One can see that directly measured velocities in VCSs and the transformed velocity along the z direction have similar shapes. The reason is that velocities in VCSs are along laser beams of laser heads whose directions are close to that of the defined z direction in the MCS.

3.4. Results of DNF and UMS identification of the turbine blade

Data acquisition of 3D CSLDV measurement has a sampling frequency of $f_{sa} = 8{,}000$ Hz. As a result, the total number of 3D CSLDV measurement points is $k = 0.5 \times 8000 \times 33 = 132{,}000$, where 33 denotes the number of scan lines. Comparisons between the consumed test time and the number of scanned points by the 3D CSLDV system and those by the 3D SLDV system are made in this work. It can be seen from Table 1 that a total of 85 measurement points were scanned by the 3D SLDV system in 900 s, while 132,000 points were scanned by the 3D CSLDV system in 115.5 s, which means that the 3D CSLDV system has much higher efficiency than the 3D SLDV system in identifying 3D modal parameters of the turbine blade. Frequency spectra of the turbine blade from the two systems are shown as black solid lines in Figs. 11 and 12, respectively, where the first six DNFs of the turbine blade shown as red dashed lines can be identified in the frequency range from 0 to 3000 Hz. Note that amplitudes of frequency spectra are different since different excitation signals are used in SLDV and CSLDV measurements. Comparison between the first six DNFs of the turbine blade identified from measurement by the 3D CSLDV system and those by the SLDV system are shown in Table 2. Differences between the first six DNFs identified by the two systems are less than 1.5%.

The procedure of identifying the x component of the mode shape of

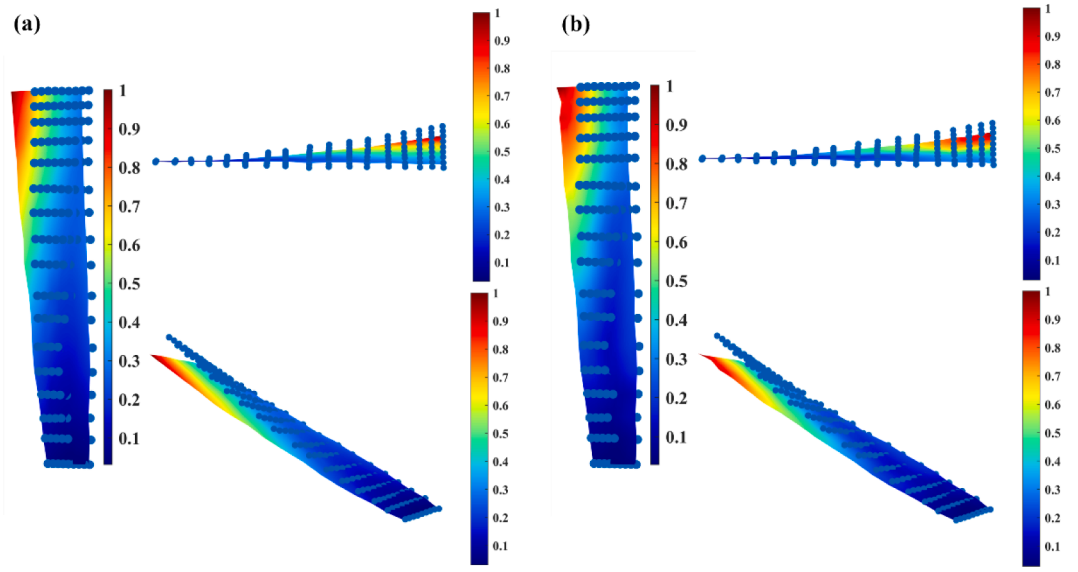

Fig. 16. (a) Estimated third FF-DMSs of the turbine blade using the 3D SLDV system and (b) corresponding FF-UMSs using the 3D CSLDV system, with views from three different angles.

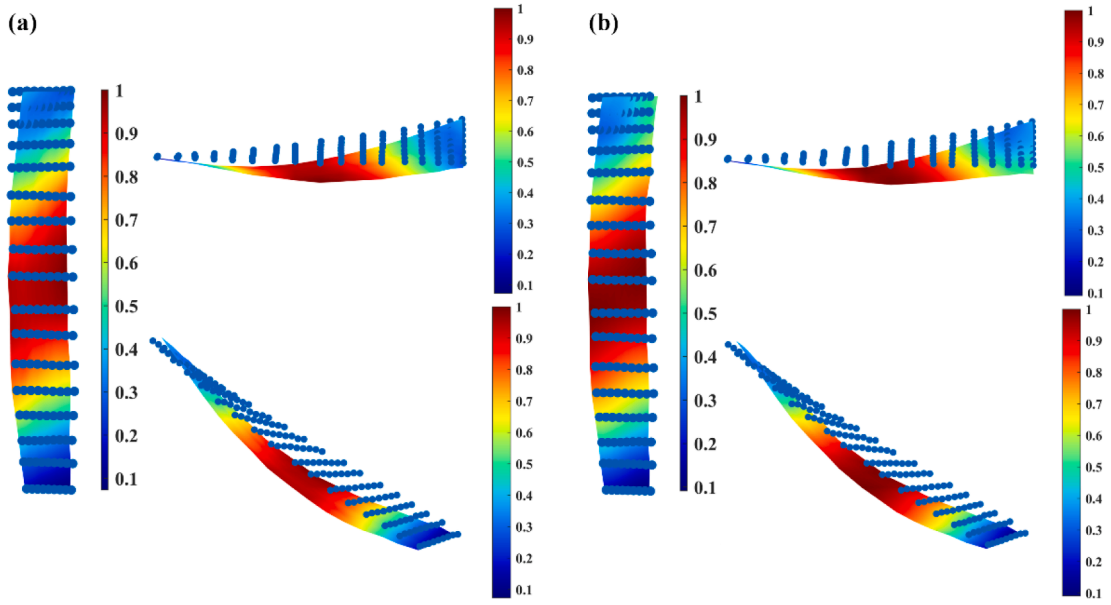

Fig. 17. (a) Estimated fourth FF-DMSs of the turbine blade using the 3D SLDV system and (b) corresponding FF-UMSs using the 3D CSLDV system, with views from three different angles.

the turbine blade at its third damped natural frequency of 399 Hz, which can be obtained from the third peak in the frequency spectrum in Fig. 12, is used to explain details of the EDM introduced in Section 2. The first step, as shown in Figs. 13(a) and 13(b), is to conduct a three-time averaging on response of each scan line, and to obtain the i-th DNF $\omega_{d,i}$ of the turbine blade by processing its averaged vibration component in the x direction of the MCS via FFT and a peak-picking process on its averaged frequency spectrum. The following step is to filter raw response in the first step using its identified DNF. In this case, the third DNF of 399 Hz is selected, and the used filter has a passband of 398 to 400 Hz. The frequency spectrum shown in Fig. 13(c) is filtered response. The final step is to multiply filtered response from the second step by sinusoidal signals $\cos(\omega_{d,i}t)$ and $\sin(\omega_{d,i}t)$, where $\omega_{d,i}$ is the identified DNF, and apply a low-pass filter with a cutoff frequency of 1 Hz to multiplied response to remove $\sin(2\omega_{d,i}t)$ and $\cos(2\omega_{d,i}t)$ in Eqs. (12) and (13), respectively, to obtain the i-th UMS of the turbine blade. The normalized x component of the third UMS of the turbine blade using a unit maximum absolute component value can be seen in Fig. 13(d).

The first six 3D FF-UMSs of the model turbine blade estimated by the 3D CSLDV system and corresponding full-field damped mode shapes (FF-DMSs) estimated by the 3D SLDV system can be found in Figs. 14-19, where left ones are FF-DMSs estimated by the 3D SLDV system and right ones are FF-UMSs estimated by the 3D CSLDV system. Mode shapes are normalized by the maximum values of their corresponding modes, respectively, and shown in views from three different angles. DMSs of the turbine blade estimated by the 3D SLDV system can be compared with its corresponding UMSs estimated by the 3D CSLDV system since it has relatively small damping ratios. Blue points in Figs. 14-19 are selected points from the profile of the turbine blade to denote its un-deformed shape. Based on scaled deformations shown in Figs. 14-19, one

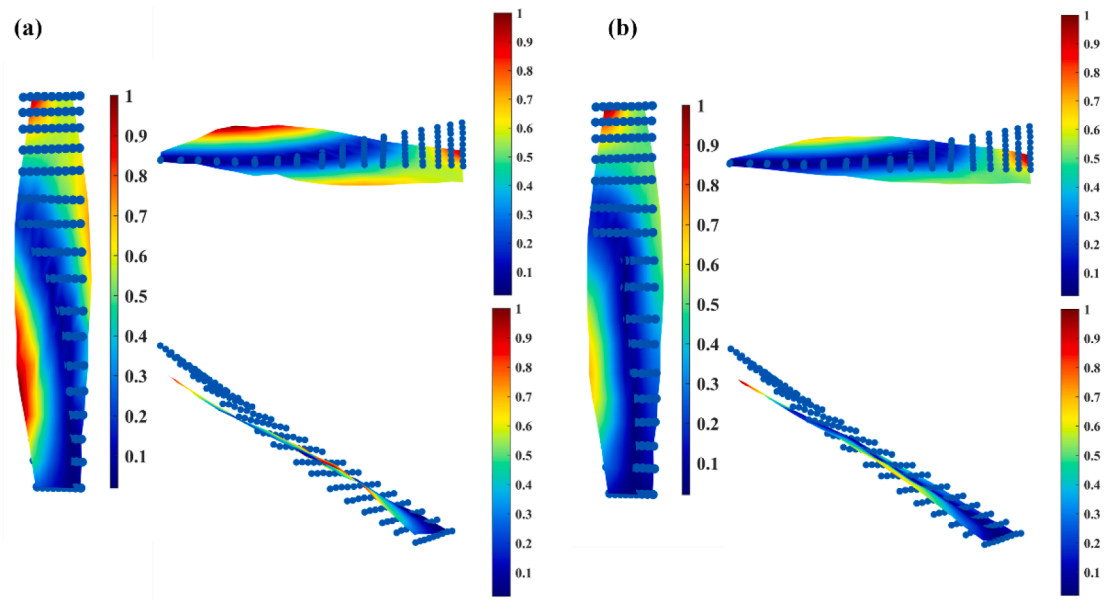

Fig. 18. (a) Estimated fifth FF-DMSs of the turbine blade using the 3D SLDV system and (b) corresponding FF-UMSs using the 3D CSLDV system, with views from three different angles.

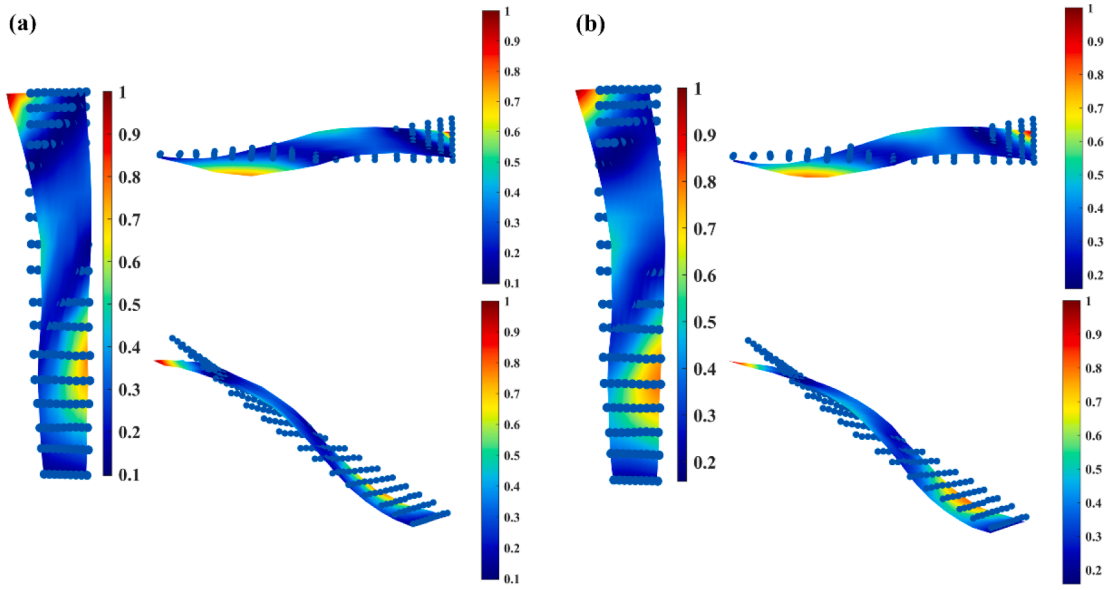

Fig. 19. (a) Estimated sixth FF-DMSs of the turbine blade using the 3D SLDV system and (b) corresponding FF-UMSs using the 3D CSLDV system, with views from three different angles.

Table 3
MAC values between 3D FF-UMSs of the turbine blade estimated by the 3D CSLDV system and corresponding FF-DMSs estimated by the 3D SLDV system.

Mode number	1	2	3	4	5	6
MAC values (%)	100	99.1	99.1	99.5	95.8	97.2

can see that the second, third, and fifth FF-UMSs estimated by the 3D CSLDV system are torsional modes and the first, fourth, and sixth FF-UMSs estimated by the 3D CSLDV system are bending modes, which are similar to corresponding FF-DMSs estimated by the 3D SLDV system. Mode shapes from both systems have much smaller deformations along the *y* direction than the other two directions, since it is more difficult to excite longitudinal vibration of a cantilever structure than its transverse vibration; this is consistent with results of 3D real-time response shown in Fig. 10. Another possible reason is that arrangement of three laser heads is close to a plane instead of a cone, which leads to a slightly smaller response amplitude along the *y* direction. MAC values [42] between 3D FF-UMSs of the turbine blade estimated by the 3D CSLDV system and its FF-DMSs estimated by the 3D SLDV system are calculated and shown in Table 3. One can see that MAC values between mode shapes estimated by the two systems have a minimum value of 95% for all the six modes, showing high correlations and the same level of accuracy between estimated mode shapes from the proposed 3D CSLDV system and the commercial 3D SLDV system.

4. Conclusions

DNFs and 3D FF-UMSs of a clamped-free model turbine blade with a

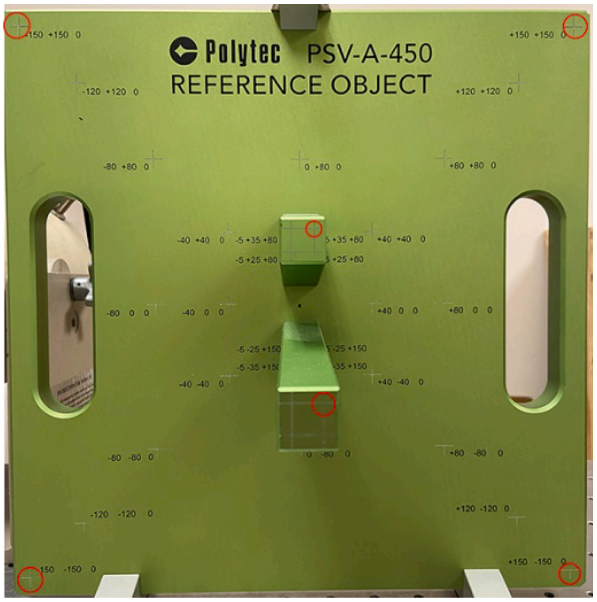

Fig. A1. Details of the reference object and points marked by red circles for calibration purposes.

curved surface under random excitation are identified by a novel general-purpose 3D CSLDV system via the EDM. Three laser heads, an external controller, and a profile scanner are used to build the 3D CSLDV system. In order to ensure that three laser spots can synchronously and continuously move along the same scan trajectory, spatial relations among the three laser heads are determined via a calibration procedure, and used with the 3D profile of the turbine blade to design a 3D full-field trajectory to scan its surface. The first six modal parameters of the turbine blade identified from measurement by the 3D CSLDV system are compared with those by the SLDV system. Differences between the first six DNFs identified by the two systems are less than 1.5%, and MAC values between mode shapes estimated by the two systems have a minimum value of 95.8% for all the six modes, indicating that the 3D CSLDV system proposed in this study have the same accuracy as that of the commercial 3D SLDV system in modal parameter estimation. In modal testing of the turbine blade, the number of points scanned by the 3D CSLDV system is about 1,500 times that by the 3D SLDV system, while the consumed test time by the 3D CSLDV system is less than 1/8 of that by the 3D SLDV system, which means that the 3D CSLDV system has much higher efficiency in identifying 3D modal parameters of the turbine blade than the 3D SLDV system.

CRediT authorship contribution statement

K. Yuan: Methodology, Software, Validation, Writing – original draft. **W.D. Zhu:** Conceptualization, Methodology, Supervision, Validation, Funding acquisition, Writing – review & editing.

Declaration of Competing Interest

The authors declare that they have no known competing financial interests or personal relationships that could have appeared to influence the work reported in this paper.

Data availability

Data will be made available on request.

Acknowledgement

The authors would like to acknowledge the support from the National Science Foundation under Grant No. 1763024.

Appendix

When any two arbitrary points are selected from the reference object, the spatial distance between them keeps constant in any two different coordinate systems. For two reference points in coordinate systems MCS and VCS defined in this study, it can be written as

$$\left|\mathbf{P}^m_{MCS}-\mathbf{P}^n_{MCS}\right| = \left|\mathbf{P}^m_{VCS}-\mathbf{P}^n_{VCS}\right| \tag{A1}$$

By assuming that a total number of H ($H \geq 4$) points are selected for calibration, m is from 1 to $H-1$ and n is from $m+1$ to H. An over-determined nonlinear problem with $H(H-1)/2$ equations like Eq. (A1) can be solved to obtain exact values of r via the nonlinear least squares method, in which initial values of r can be inputted using roughly measured distances from incident points of laser beams on the X mirror to selected points. Six points with coordinates (-150,150,0), (150,150,0), (150,-150,0), (-150,-150,0), (-5,25,80), and (-5,-35,150) are selected from four corners and two poles of the reference object, as shown in Fig. A1. The matrices **R** and **T** can be solved via the following optimization problem:

$$F(\mathbf{T},\mathbf{R}) = \delta = \min \sum_{m=1}^{H} \left|\mathbf{P}^m_{MCS} - \left(\mathbf{T} + \mathbf{R}\mathbf{P}^m_{VCS}\right)\right| \tag{A2}$$

In the MCS, let $\bar{\mathbf{P}}_{MCS} = \left(\sum_{m=1}^{H}\mathbf{P}^m_{MCS}\right)/H$, $\mathbf{q}^m_{MCS} = \mathbf{P}^m_{MCS} - \bar{\mathbf{P}}_{MCS}$, and $\mathbf{Q}_{MCS} = [\mathbf{q}^1_{MCS}, \mathbf{q}^2_{MCS}, \ldots, \mathbf{q}^H_{MCS}]$. Similarly, in the VCS, $\mathbf{Q}_{VCS} = [\mathbf{q}^1_{VCS}, \mathbf{q}^2_{VCS}, \ldots, \mathbf{q}^H_{VCS}]$ can be constructed by $\bar{\mathbf{P}}_{VCS} = \left(\sum_{m=1}^{H}\mathbf{P}^m_{VCS}\right)/H$ and $\mathbf{q}^m_{VCS} = \mathbf{P}^m_{VCS} - \bar{\mathbf{P}}_{VCS}$. A 3×3 matrix **A** can be obtained by $\mathbf{A} = \mathbf{Q}_{VCS}\mathbf{Q}^{\mathrm{T}}_{MCS}$, and can also be decomposed through the singular value decomposition $\mathbf{A} = \mathbf{U}\Sigma\mathbf{V}^{\mathrm{T}}$, where **U** and **V** are two 3×3 orthogonal matrices, and **Σ** is a 3×3 diagonal matrix with non-negative real numbers on the diagonal. One can use **U** and **V** to obtain **R** and **T** via

$$\mathbf{R} = \mathbf{V}\begin{bmatrix} 1 & 0 & 0 \\ 0 & 1 & 0 \\ 0 & 0 & \left|\mathbf{V}\mathbf{U}^{\mathrm{T}}\right| \end{bmatrix}\mathbf{U}^{\mathrm{T}} \tag{A3}$$

and

$$\mathbf{T} = \bar{\mathbf{P}}_{MCS} - \mathbf{R}\bar{\mathbf{P}}_{VCS} \tag{A4}$$

References

[1] S.J. Rothberg, M.S. Allen, P. Castellini, D. Di Maio, J.J.J. Dirckx, D.J. Ewins, B. J. Halkon, P. Muyshondt, N. Paone, T. Ryan, H. Steger, E.P. Tomasini, S. Vanlanduit, J.F. Vignola, An international review of laser Doppler vibrometry: Making light work of vibration measurement, Opt. Lasers Eng. 99 (2017) 11–22.

[2] P. Castellini, M. Martarelli, E.P. Tomasini, Laser Doppler vibrometry: Development of advanced solutions answering to technology's needs, Mech. Syst. Sig. Process. 20 (6) (2006) 1265–1285.

[3] M. Rajaram Narayanan, S. Nallusamy, Analysis on vibration characteristics of wind turbine blade to improve the effectiveness through CFD developed by ANSYS, Material Science, Forum 937 (2018) 43–50.

[4] M. Rajaram Narayanan, S. Nallusamy and R. Sathiyan, Design and analysis of a wind turbine blade with dimples to enhance the efficiency through CFD with ANSYS R16.0, MATEC Web of Conference, 207(2004) (2018) 01-05.

[5] J. La, J. Choi, S. Wang, K. Kim, K. Park, Continuous scanning laser Doppler vibrometer for mode shape analysis, Opt. Eng. 42 (3) (2003) 730–737.

[6] C.X. Qu, T.H. Yi, H.N. Li, B. Chen, Closely spaced modes identification through modified frequency domain decomposition, Measurement 128 (2018) 388–392.

[7] C.X. Qu, T.H. Yi, Y.Z. Zhou, H.N. Li, Y.F. Zhang, Frequency identification of practical bridges through higher-order spectrum, J. Aerosp. Eng. 31 (3) (2018) 04018018.

[8] C.X. Qu, T.H. Yi, H.N. Li, Mode identification by eigensystem realization algorithm through virtual frequency response function, Struct. Control Health Monit. 26 (10) (2019) e2429.

[9] P. Margerit, T. Gobin, A. Lebée, J.F. Caron, The robotized laser doppler vibrometer: On the use of an industrial robot arm to perform 3D full-field velocity measurements, Opt. Lasers Eng. 137 (2021), 106363.

[10] P. O'Malley, T. Woods, J. Judge, J. Vignola, Five-axis scanning laser vibrometry for three-dimensional measurements of non-planar surfaces, Meas. Sci. Technol. 20 (11) (2009), 115901.

[11] S. Sels, S. Vanlanduit, B. Bogaerts, R. Penne, Three-dimensional full-field vibration measurements using a handheld single-point laser Doppler vibrometer, Mech. Syst. Sig. Process. 126 (2019) 427–438.

[12] D. Kim, H. Song, H. Khalil, J. Lee, S. Wang, K. Park, 3-D vibration measurement using a single laser scanning vibrometer by moving to three different locations, IEEE Trans. Instrum. Meas. 63 (8) (2014) 2028–2033.

[13] D.M. Chen, W.D. Zhu, Investigation of three-dimensional vibration measurement by a single scanning laser Doppler vibrometer, J. Sound Vib. 387 (2017) 36–52.

[14] T. Miyashita, Y. Fujino, Development of 3D vibration measurement system using laser doppler vibrometers, In Health Monitoring and Smart Nondestructive Evaluation of Structural and Biological Systems V 6177 (2006) 170–179.

[15] W. Xu, W.D. Zhu, S.A. Smith, M.S. Cao, Structural damage detection using slopes of longitudinal vibration shapes, J. Vib. Acoust. 138 (3) (2016), 034501.

[16] K. Yuan, W. Zhu, Modeling of welded joints in a pyramidal truss sandwich panel using beam and shell finite elements, J. Vib. Acoust. 143 (4) (2021), 041002.

[17] Y. Chen, A.S.E. Mendoza, D.T. Griffith, Experimental and numerical study of high-order complex curvature mode shape and mode coupling on a three-bladed wind turbine assembly, Mech. Syst. Sig. Process. 160 (2021), 107873.

[18] C. Vuye, S. Vanlanduit, F. Presezniak, G. Steenackers, P. Guillaume, Optical measurement of the dynamic strain field of a fan blade using a 3D scanning vibrometer, Opt. Lasers Eng. 49 (7) (2011) 988–997.

[19] K. Bendel, M. Fischer, M. Schuessler, Vibrational analysis of power tools using a novel three-dimensional scanning vibrometer, in: Sixth International Conference on Vibration Measurements by Laser Techniques: Advances and Applications, 5503, International Society for Optics and Photonics, 2004, pp. 177–184.

[20] B.J. Halkon, S.R. Frizzel, S.J. Rothberg, Vibration measurements using continuous scanning laser vibrometry: velocity sensitivity model experimental validation, Meas. Sci. Technol. 14 (6) (2003) 773.

[21] D. Di Maio, P. Castellini, M. Martarelli, S. Rothberg, M.S. Allen, W.D. Zhu, D. J. Ewins, Continuous Scanning Laser Vibrometry: A raison d'être and applications to vibration measurements, Mech. Syst. Sig. Process. 156 (2021), 107573.

[22] L.F. Lyu, W.D. Zhu, Operational modal analysis of a rotating structure under ambient excitation using a tracking continuously scanning laser Doppler vibrometer system, Mech. Syst. Sig. Process. 152 (2021), 107367.

[23] L.F. Lyu, W.D. Zhu, Operational modal analysis of a rotating structure subject to random excitation using a tracking continuously scanning laser Doppler vibrometer via an improved demodulation method, J. Vib. Acoust. 144 (1) (2022), 011006.

[24] D.M. Chen, Y. Xu, W. Zhu, Damage identification of beams using a continuously scanning laser Doppler vibrometer system, J. Vib. Acoust. 138 (5) (2016), 051011.

[25] D.M. Chen, Y. Xu, W. Zhu, Experimental investigation of notch-type damage identification with a curvature-based method by using a continuously scanning laser Doppler vibrometer system, J. Nondestr. Eval. 36 (2) (2017) 38.

[26] D.M. Chen, Y. Xu, W. Zhu, Identification of damage in plates using full-field measurement with a continuously scanning laser Doppler vibrometer system, J. Sound Vib. 422 (2018) 542–567.

[27] Y.F. Xu, D.M. Chen, W.D. Zhu, Operational modal analysis using lifted continuously scanning laser Doppler vibrometer measurements and its application to baseline-free structural damage identification, J. Vib. Control 25 (7) (2019) 1341–1364.

[28] B. Weekes, D. Ewins, Multi-frequency, 3D ODS measurement by continuous scan laser Doppler vibrometry, Mech. Syst. Sig. Process. 58 (2015) 325–339.

[29] D.M. Chen, W. Zhu, Investigation of three-dimensional vibration measurement by three scanning laser Doppler vibrometers in a continuously and synchronously scanning mode, J. Sound Vib. 498 (2021), 115950.

[30] K. Yuan, W. Zhu, Estimation of modal parameters of a beam under random excitation using a novel 3D continuously scanning laser Doppler vibrometer system and an extended demodulation method, Mech. Syst. Sig. Process. 155 (2021), 107606.

[31] K. Yuan, W. Zhu, In-plane operating deflection shape measurement of an aluminum plate using a three-dimensional continuously scanning laser Doppler vibrometer system, Exp. Mech. 62 (2022) 667–676.

[32] K. Yuan, W. Zhu, A novel general-purpose three-dimensional continuously scanning laser Doppler vibrometer system for full-field vibration measurement of a structure with a curved surface, J. Sound Vib. 540 (2022), 117274.

[33] A.B. Stanbridge, D.J. Ewins, Modal testing using a scanning laser Doppler vibrometer, Mech. Syst. Sig. Process. 13 (2) (1999) 255–270.

[34] A.B. Stanbridge, D.J. Ewins, A.Z. Khan, Modal testing using impact excitation and a scanning LDV, Shock Vib. 7 (2) (2000) 91–100.

[35] M.S. Allen, M.W. Sracic, A new method for processing impact excited continuous-scan laser Doppler vibrometer measurements, Mech. Syst. Sig. Process. 24 (3) (2010) 721–735.

[36] S. Vanlanduit, P. Guillaume, J. Schoukens, Broadband vibration measurements using a continuously scanning laser vibrometer, Meas. Sci. Technol. 13 (10) (2002) 1574–1582.

[37] D. Di Maio, D.J. Ewins, Continuous Scan, a method for performing modal testing using meaningful measurement parameters, Part I, Mechanical Systems and Signal Processing 25 (8) (2011) 3027–3042.

[38] S. Yang, M.S. Allen, Output-only modal analysis using continuous-scan laser Doppler vibrometry and application to a 20 kW wind turbine, Mech. Syst. Sig. Process. 31 (2012) 228–245.

[39] L.F. Lyu, W.D. Zhu, Full-field mode shape estimation of a rotating structure subject to random excitation using a tracking continuously scanning laser Doppler vibrometer via a two-dimensional scan scheme, Mech. Syst. Sig. Process. 169 (2022) 108532.

[40] K.S. Arun, T.S. Huang, S.D. Blostein, Least-squares fitting of two 3-D point sets, IEEE Trans. Pattern Anal. Mach. Intell. 5 (1987) 698–700.

[41] L. Meirovitch, Analytical methods in vibrations, The Macmillan Co, 1967.

[42] D.J. Ewins, Modal Testing: Theory, Practice, and Application, 2nd ed., Research Studies Press Ltd., Hertfordshire, UK, 2000.